Ecotoxicology and Environmental Safety 254 (2023) 114718

Contents lists available at ScienceDirect

Ecotoxicology and Environmental Safety

journal homepage: www.elsevier.com/locate/ecoenv

Review

Fluoride exposure disrupts the cytoskeletal arrangement and ATP synthesis of HT-22 cell by activating the RhoA/ROCK signaling pathway

Lingli Chen [a,b,1], Penghuan Jia [a,1], Yuye Liu [a], Rui Wang [a], Zhihong Yin [a], Dongfang Hu [a], Hongmei Ning [a], Yaming Ge [a,*]

[a] College of Animal Science and Veterinary Medicine, Henan Institute of Science and Technology, Xinxiang, Henan Provence 453003, China
[b] Postdoctoral Research and Development Base, Henan Institute of Science and Technology, Xinxiang, Henan Provence 453003, China

ARTICLE INFO

Editor: Professor Bing Yan

Keywords:
Fluorine
Neurotoxicology
RhoA/ROCK/LIMK/Cofilin signaling pathway
Actin homeostasis
ATP/ATPase

ABSTRACT

Background: Fluoride, an environmental contaminant, is ubiquitously present in air, water, and soil. It usually enters the body through drinking water and may cause structural and functional disorders in the central nervous system in humans and animals. Fluoride exposure affects cytoskeleton and neural function, but the mechanism is not clear.

Methods: The specific neurotoxic mechanism of fluoride was explored in HT-22 cells. Cellular proliferation and toxicity detection were investigated by CCK-8, CCK-F, and cytotoxicity detection kits. The development morphology of HT-22 cells was observed under a light microscope. Cell membrane permeability and neurotransmitter content were determined using lactate dehydrogenase (LDH) and glutamate content determination kits, respectively. The ultrastructural changes were detected by transmission electron microscopy, and actin homeostasis was observed by laser confocal microscopy. ATP enzyme and ATP activity were determined using the ATP content kit and ultramicro-total ATP enzyme content kit, respectively. The expression levels of GLUT1 and 3 were assessed by Western Blot assays and qRT-PCR.

Results: Our results showed that fluoride reduced the proliferation and survival rates of HT-22 cells. Cytomorphology showed that dendritic spines became shorter, cellular bodies became rounder, and adhesion decreased gradually after fluoride exposure. LDH results showed that fluoride exposure increased the membrane permeability of HT-22 cells. Transmission electron microscopy results showed that fluoride caused cells to swell, microvilli content decreased, cellular membrane integrity was damaged, chromatin was sparse, mitochondria ridge gap became wide, and microfilament and microtubule density decreased. Western Blot and qRT-PCR analyses showed that RhoA/ROCK/LIMK/Cofilin signaling pathway was activated by fluoride. F-actin/G-actin fluorescence intensity ratio remarkably increased in 0.125 and 0.5 mM NaF, and the mRNA expression of MAP2 was significantly decreased. Further studies showed that GLUT3 significantly increased in all fluoride groups, while GLUT1 decreased ($p < 0.05$). ATP contents remarkably increased, and ATP enzyme activity substantially decreased after NaF treatment with the control.

Conclusion: Fluoride activates the RhoA/ROCK/LIMK/Cofilin signaling pathway, impairs the ultrastructure, and depresses the connection of synapses in HT-22 cells. Moreover, fluoride exposure affects the expression of glucose transporters (GLUT1 and 3) and ATP synthesis. Sum up fluoride exposure disrupts actin homeostasis, ultimately affecting structure, and function in HT-22 cells. These findings support our previous hypothesis and provide a new perspective on the neurotoxic mechanism of fluorosis.

1. Introduction

Fluorine (F) is widespread in the environment, rock (0–3400 mg/kg), soil (20–700 mg/kg), water, plant, and animal body (20–700 mg/kg) in various concentrations (Zhang et al., 2019). The U.S. Environmental Protection Agency established of maximum contaminant level (MCL) for F in drinking water of 4 mg/L and a secondary MCL (SMCL) of 2 mg/L (U.S. Environmental Protection Agency, 2010), The World Health

* Corresponding author.
E-mail address: ndgeyaming@126.com (Y. Ge).
[1] Equal contribution to this work.

https://doi.org/10.1016/j.ecoenv.2023.114718
Received 29 October 2022; Received in revised form 25 February 2023; Accepted 28 February 2023
Available online 10 March 2023

Table 1
The primer sequences of qRT-PCR.

Gene name	Accession No.	Primer sequences (5′–3′)
RhoA	JN971019.1	F: CCTTCGGAATGACGAGCAC R: AGATGAGGCACCCAGACTTTT
ROCK 1	NP_033097.1	F: ACCCACCATCTGGCTTTGTC R: CGGTTTATCAGGTAGCATCCC
ROCK 2	NP_033098.2	F: GATGGTTGTCATTGCCTGTGC R: TGCTCTTTATCTTGTTCGCTGT
Cofilin	D00472.1	F: CAGACTGTGGACGACCCCTA R: GCTCTTGAGGGGTGCATTCT
LIMK	U15159	F: TGCAGTATTGACACGTCCCC R: TCGGTGTGTCACCTTGATGG
MAP2	M 21041	F: CAGCAGAGGTCCCAAGTGAG R: GAAACAAGCAGGTCGGAGAT
Tau	NM_001038609.2	F: CCCTCTAATCCACTGGCACAT R: GAAGTCTGAAGGCTCATAAA
GLUT1	NM_011400.3	F: CGGCCTGACTACTGGCTTTG R: AAGCCAAACACCTGGGCAAT
GLUT3	AH005389.3	F: CGCATGAGGGCACAAATGTC R: GGGTGGCATCTAATCCTGGG
GAPDH	GU214026	F: CCTTCCGTGTTCCTACCC R: GCCCTCAGATGCCTGCT

Organization (WHO, 2017) established a guideline for F in drinking water of 1.5 mg/L. The clinical application indicates that fluoride prevents dental caries by reducing the demineralization of enamel (Wang et al., 2022). Therefore, fluoride is used for the treatment of dental caries, either systemically or topically in the last few years (Whelton et al., 2019). However, the persistent toxic effect of fluorine in humans and animals caused by excessive intake, and the potential toxic mechanisms in the CNS is one of great concern for public health. F^- can cross the blood-brain barrier and result in an increased deposition in the brain of Wistar rats, resulting in high levels of epinephrine, histamine, serotonin, and glutamate and decreased levels of norepinephrine, acetylcholine, and dopamine (Reddy et al., 2021). Consequently, it may result in changes in cell activity, and ion transport at the cellular level (Dec et al., 2017). Epidemiological findings have demonstrated that exposure to fluoride induces developmental neurotoxicity and motor disorders in male Wistar rats (Oyagbemi et al., 2020), impairs the learning and memory abilities of the male Sprague–Dawley rat offspring, reduces dendritic spine density, lower postsynaptic density protein-95 (PSD95) and synaptophysin expression in the hippocampus (Zhu et al., 2011; Li et al., 2022). Studies showed that excessive endoplasmic reticulum stress, neuronal apoptosis, autophagy, cytoskeletal damage, and synaptic impairment occur in rat offspring following exposure to NaF (Chen et al., 2018, 2017; Niu et al., 2018; Wu et al., 2015; Zhu et al., 2017). Fluoride exposure causes disorder of microtubule construction and degeneration of axons dendrites in Purkinje cells (Oyagbemi et al., 2020). Fluoride exposure can promote nuclear chromatin lysis in glial cells and reduce Nissl body content, ribosomal, and RNA concentrations in brain gray matter neurons resulting in neuronal aging, and degeneration (Yan et al., 2016). Therefore, fluoride exposure can cause structural and functional damage to the nervous system, and induce the

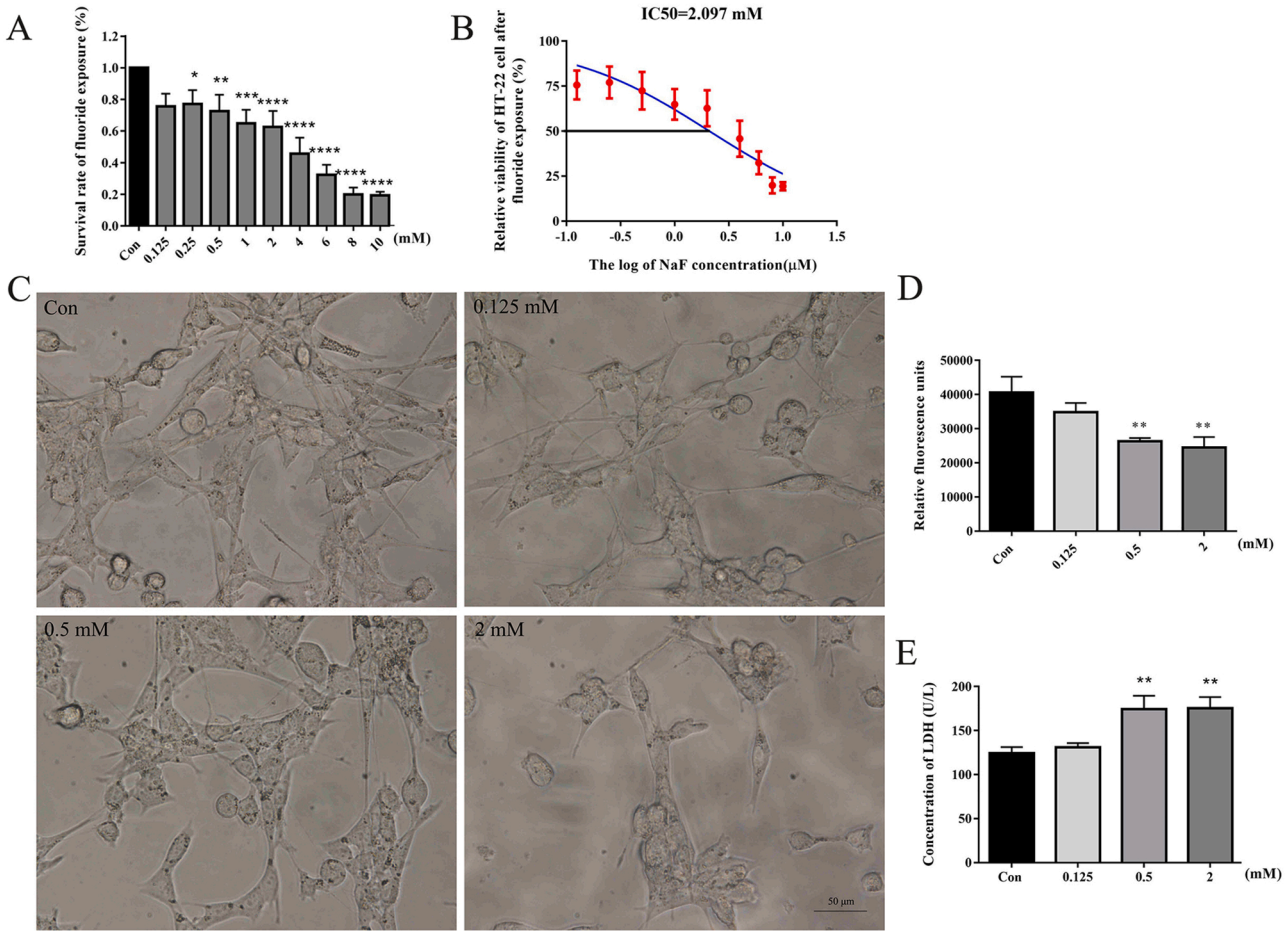

Fig. 1. Fluoride affects the proliferation, morphology and membrane permeability of HT-22 cells. A: fluoride depressing HT-22 cell proliferation; B: Determination of half maximal inhibitory concentration (IC50) of fluoride in HT-22 cell; C: Morphological change after fluoride exposure; D: CCK-F kit for the detection of live cell fluorescence intensity; E: Determination of LDH content in cell culture supernatant after fluoride exposure for 24 h. *Significantly different from control ($p < 0.05$), * *Highly significant differences from control ($p < 0.01$), * **Remarkable significant differences from control ($p < 0.001$), * ** *Extremely significant differences from control ($p < 0.0001$).

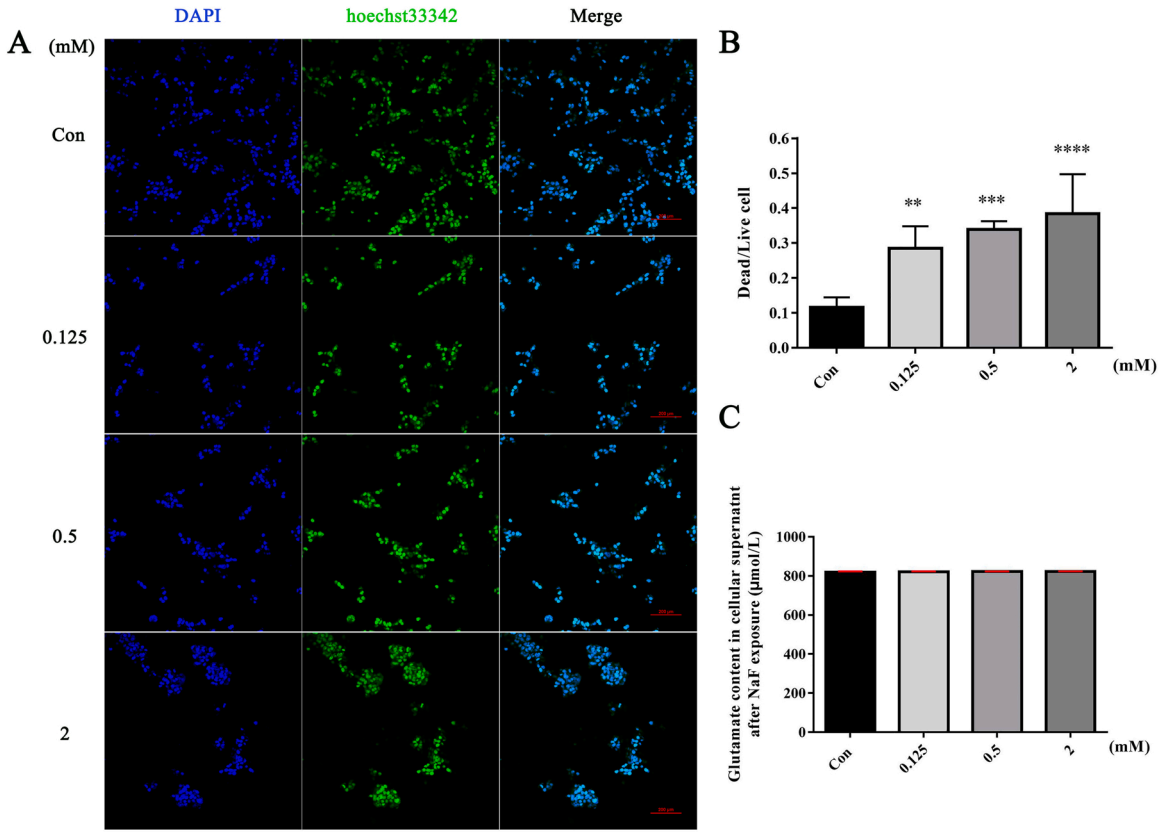

Fig. 2. Effects of fluoride on the dead/live rate and glutamate release capacity in HT-22 cell. A: Detection of dead/live rate in HT-22 cell using the cytotoxicity detection kit; B: Statistical result of cytotoxicity detection; C: Determination of the content of glutamate in cell culture supernatant after NaF exposure for 24 h. *Significantly different from control ($p < 0.05$), * *Highly significant differences from control ($p < 0.01$), ** *Remarkable significant differences from control ($p < 0.001$), * ** *Extremely significant differences from control ($p < 0.0001$).

learning and memory abilities to decline in humans and animals.

The Rho GTPase/Rho kinase (ROCK) signaling pathway plays an important role in the modulation of cell cytoskeleton (Rao et al., 2017; Amano et al., 2010; Sun et al., 2022). Rho GTPase activates its effector molecules, ROCK1 and ROCK2, and regulates diverse signaling effectors and pathophysiological processes (e.g, cell division, cell migration, wound healing, or immune surveillance) (Hauke et al., 2022). α-Crystallin could counteract the effect of regeneration inhibitory factors and stimulate axonal regeneration by mediating the RhoA/ROCK signaling pathway (Wang et al., 2012). RhoA/ROCK signaling may couple or coordinate actomyosin dynamics with mitochondrial dynamics to achieve optimal actomyosin function, leading to protrusive and migratory behavior (Qu et al., 2022). In the SD rat model, METH treatment increased the blood-brain barrier permeability by activating the RhoA/ROCK pathway, resulting in F-actin cytoskeleton rearrangement and downregulation of tight junction proteins (Xue et al., 2019). The effectors of the different RhoA usually have opposing effects on downstream pathways (Shamah et al., 2001). ROCK1 and 2 inhibit the myosin light chain phosphatase complex of type 1 (MYPT1), thereby modifying the actin-cytoskeletal dynamics. In addition, LIM domain kinase 1 (LIMK1) and its paralogue LIMK2, one of the downstream effectors of ROCKs, are two closely related kinases that control actin cytoskeleton dynamics (Berrou et al., 2022). RhoA stabilizes the stress fibers and prevents the depolymerization of actin filaments through Cofilin phosphorylation, and ROCK1 and 2 activate LIMKs thus inhibiting Cofilin, and resulting in actin polymerization (Lee et al., 2022). The RhoA/ROCK/LIMK/Cofilin pathway modulates actin assembly in various cellular cell types in response to extracellular stimuli (Ohashi, 2015).

The microtubule-associated proteins (MAPs) are a family of homologous proteins, including MAP2 and MAP4, with three or four basic microtubule-binding domains in their carboxy-terminal regions (Sündermann et al., 2016). Tau protein (MAPT) is classified as a MAP, it regulates the axonal microtubule arrangement, promotes the assembly and interaction of microtubules with the cytoskeleton, impinges on axonal transport and synaptic plasticity (Sündermann et al., 2016; Brandt et al., 2020). Tau, MAP2, and NFs (nerve fibers) are essential for maintaining the stability of the cytoskeleton (Gutiérrez-Vargas et al., 2022). Actin, which is present in all eukaryotic species and cell types, is the major protein in myofibrillar filaments and regulates various cell functions, such as muscle contraction, cell motility, and cell division (Pandey et al., 2006). Actin exists as a dynamic equilibrium mixture of two forms namely polymeric filamentous actin (F-actin) and monomeric globular actin (G-actin) (Ohno et al., 2013), which control the polymerization and depolymerization of actin filaments, and formation of actin-based bundles and cellular protrusions (Yamaguchi and Condeelis, 2007). F-actin could be depolymerized into G-actin, and ATP can accelerate this transformation process (Zhou et al., 2018). Under normal conditions, the transformation between F-actin and G-actin maintains a dynamic balance. However, cellular structure is damaged when this balance is disturbed (Turner, 2009; Song et al., 2019). Liu et al. found that F-actin/G-actin, CA1 spine density, and synapse density remarkably decreased in female C57BL/6 mice hippocampus after letrozole treatment, in which actin dynamic balance caused damage (Liu et al., 2019).

Glucose transporters (GLUTs) play a pivotal role in multi-systematic functions in humans and animals. The high energy demand of the brain mainly depends on the D-glucose supply from the blood through the glucose transporters in the capillaries and brain cells (Koepsell, 2020). GLUTs are responsible for the cellular uptake of hexoses (Wang et al., 2022), and 14 types have been studied, including GLUT1 and GLUT3, which are preferentially expressed in the brain (Maher and Simpson,

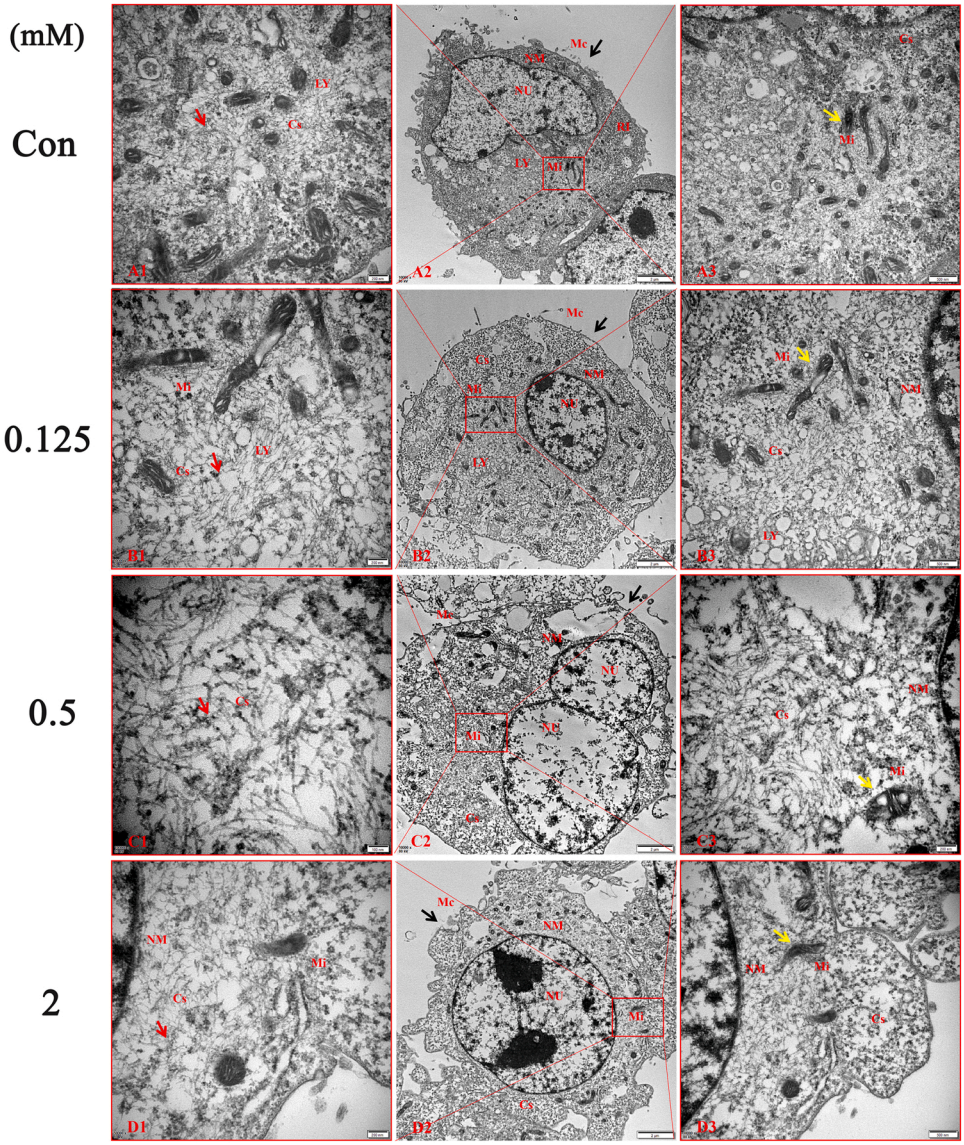

Fig. 3. Fluoride exposure impaired the ultrastructure in HT-22 cells. A1–3, Control group; B1–3, 0.125 mM fluoride group; C1–3, 0.5 mM fluoride group; D1–3, 2 mM fluoride group. The red arrows indicate microfilament and microtubule density in A1-D1. The black arrows indicate the decrease in microvilli reduction and cell membrane discontinuity and incomplete in A2-D2; The yellow arrows indicate the mitochondria ridge gap in A3-D3. Nucleus (Nu); Mitochondria (Mi); microvilli (Mc); Nuclear membrane (NM); Lysosome (Ly); Cytoskeletons (microfilament and microtubules, Cs).

1994). GLUT1 is located on the endothelial cells of the blood-brain barrier, and it mediates the transport of glucose from the blood to the brain (Schindler and Foley, 2013). GLUT3 is ubiquitously expressed in the brain and predominantly expressed in the neurons of rodents (Koepsell, 2020). GLUT3 transports glucose much more efficiently than GLUT1, and a 6–10 folds higher abundance in GLUT3 was observed compared with GLUT1 in cultured granular neurons derived from rat cerebellum (Maher and Simpson, 1994). The downregulation of GLUT1 and GLUT3 leads to a decrease in D-glucose concentration in neurons, representing an early event during the pathogenesis of AD (Koepsell, 2020). Therefore, we aimed to determine whether the brain damage induced by fluoride exposure is related to abnormal glucose transport in humans and animals.

In the present study, we established a fluorosis model in HT-22 cells to evaluate the relationship among fluoride, RhoA/ROCK/LIMK/Cofilin signaling pathway, and glucose transportation. This study will provide a new idea for exploring the neurotoxic mechanism of fluoride.

2. Materials and methods

2.1. Chemicals

The reagents used include sodium fluoride (NaF, Tianjin Jinbei Fine Chemical Industry Co., Ltd.), glycerol, glutaraldehyde (Sigma Aldrich), phenylmethylsulfonyl fluoride (PMSF Beyotime, Shanghai), dimethyl sulfoxide (DMSO, Solarbio, Beijing), and DAPI (Solarbio, Beijing). Sodium fluoride was dissolved in double distilled water and stored at 4 ℃ until diluted before use. Cell Counting Kit 8 (CCK-8, Dalian Meilun Biotechnology Co., Ltd), Cell Fluorescence Counting Kit-F (Beyotime, Shanghai), Green dead cell nucleic acid dye, and Hoechst 33342 (KeyGen BioTECH, Nanjing).

2.2. Cell culture and drug treatment

HT-22 cell line (mouse hippocampal neurons) was obtained from the Laboratory of Neural Development at Xinxiang Medical University. Cells were cultured in Dulbecco's Modified Eagle Medium (DMEM, Procell, Hangzhou, China) with 10% fetal bovine serum (Biological Industries, China), 100 U/mL penicillin-streptomycin in a damp atmosphere of 5% (*v*/*v*) CO_2 and 95% (*v*/*v*) air at 37 ℃. HT-22 cells were plated in cell

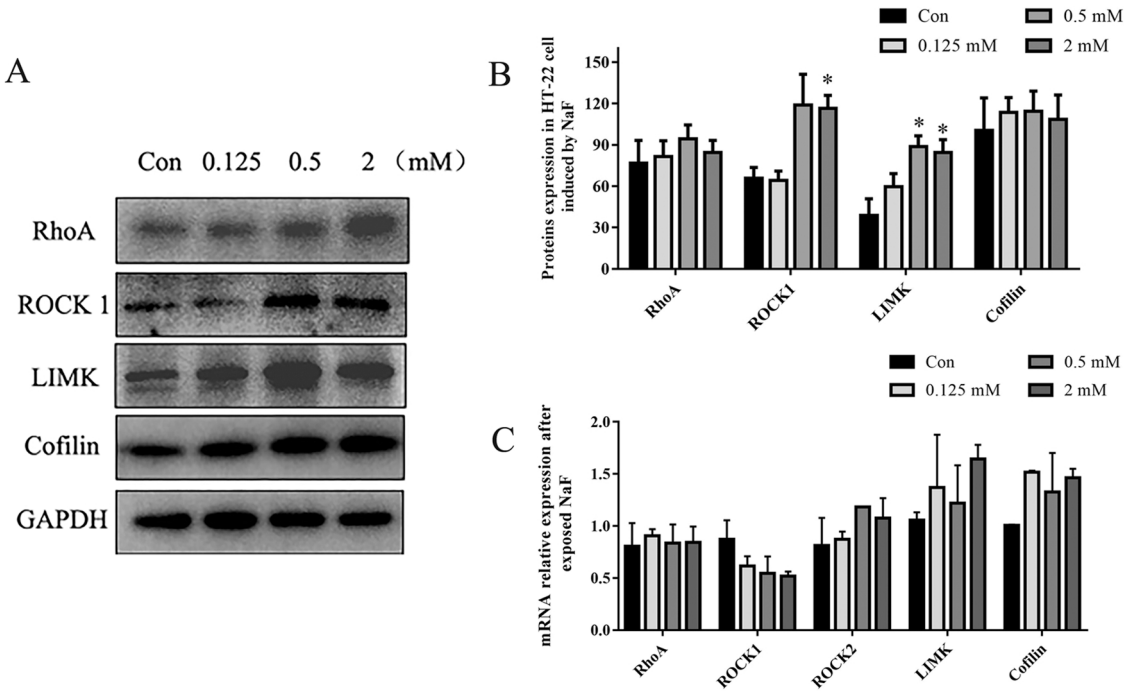

Fig. 4. Fluoride exposure activates the RhoA/ROCK/LIMK/Cofilin in HT-22 cells. A: The protein expression levels of RhoA, ROCK, LIMK, and Cofilin were determined by Western Blot; B: The statistical result of protein expression; C: mRNA expression of RhoA, ROCK, and LIMK and Cofilin. *Significantly different from control ($p < 0.05$).

culture plates after subculturing for 24 h (JET, Guangzhou, China), and then treated with diverse concentrations of sodium fluoride (0, 0.125, 0.5, 2 mM) for 24 h.

2.3. Cell proliferation assay

HT-22 cells (1×10^5 cells/100 μL) were seeded into 96-well plates and cultured in DMEM medium. Following 8 h of culture, the cells were treated with fluoride (0–10 mM) for 24 h. After the experiment, cells were treated with CCK-8, and then subcultured for 1 h. Finally, the absorbance was measured using Multiscan Spectrum (MK3, Thermo Fisher Scientific, USA) at 450 nm, and the cell survival rates were calculated.

2.4. Cell viability assay

Cell Fluorescence Counting kit-F (CCK-F) was used to detect cell activity. The treatment method in the same as that of the cell proliferation assay. Following 8 h of incubation, the cells were treated with NaF (0, 0.125, 0.5, and 2 mM) for 24 h. The medium was discarded, and the cells were treated with Calcein-AM working fluid and incubated in the dark at 37 ℃ for 30 min. Finally, the fluorescence intensity was measured in 477 nm with a fluorescence microplate reader (Thermo Fisher Scientific, USA) and analyzed using Prism software.

2.5. Cytotoxicity detection

Cells were cultured on the coverslips (diameter 14 mm), and the cells were treated with NaF (0, 0.125, 0.5, and 2 mM) for 24 h. The samples were added with green dead cell nucleic acid dye, incubated in the dark at 37 ℃ for 30 min, and added with Hoechst33342 with 4% paraformaldehyde. The samples were then incubated in the dark at room temperature for 15 min and then washed with PBS. The coverslip was placed on the slide (with an anti-fluorescence inhibitor), fluorescence microscopy was performed (Nikon, Shanghai), and results were analyzed using Prism software.

2.6. Determination of cellular membrane permeability and glutamate content

The supernatant of cells was collected after treatment with fluoride, and three repetitions were set for each group. The membrane permeability was detected using the LDH assay kit (A020–2, Nanjing Jiancheng, China) in the supernatant, and ODs were measured using the Multiscan Spectrum at 450 nm. The glutamate content determination kit (A-074–1–1, Nanjing Jiancheng, China) was used in this study, ODs were measured using the Multiscan Spectrum at 340 nm and analyzed using Prism software.

2.7. Ultrastructural observation of HT-22 cell

The ultrastructure of the HT-22 cell was observed using a transmission electron microscope. The HT-22 cell was harvested after fluoride treatment, fixed with 2.5% glutaraldehyde at room temperature, treated with 1% osmic acid, dehydrated in a graded alcohol series, and embedded in araldite resin. Sections with thicknesses of 50 nm were stained with uranyl acetate and lead citrate and then observed by TEM (H-7500, Hitachi).

2.8. F-actin/G-actin staining

Cells were cultured on the coverslips (diameter of 14 mm) in 12-well plates and then treated with NaF (0, 0.125, 0.5, and 2 mM) for 24 h. The cells were fixed in 4% formaldehyde at room temperature for 10–15 min and washed with PBS. 0.1% Triton X-100 in PBS for 5 min, washed with PBS and then added with 400 μL (9 μg/mL or 0.3 μM) of fluorescent DNase I solution (D12372, Molecular Probes, USA) per coverslip. Then the samples were incubated in the dark at 37 ℃ for 30 min and rinsed thrice with PBS to remove the unbound fluorescent solution. In total, 400 μL of phalloidin (0.5 μg/mL, P5282, Sigma) in PBS was added to the coverslip, which was then incubated in the dark at 37 ℃ for 30 min and rinsed thrice with PBS to remove unbound phalloidin. 1 × DAPI solution was incubated at room temperature for 5 min and then washed with

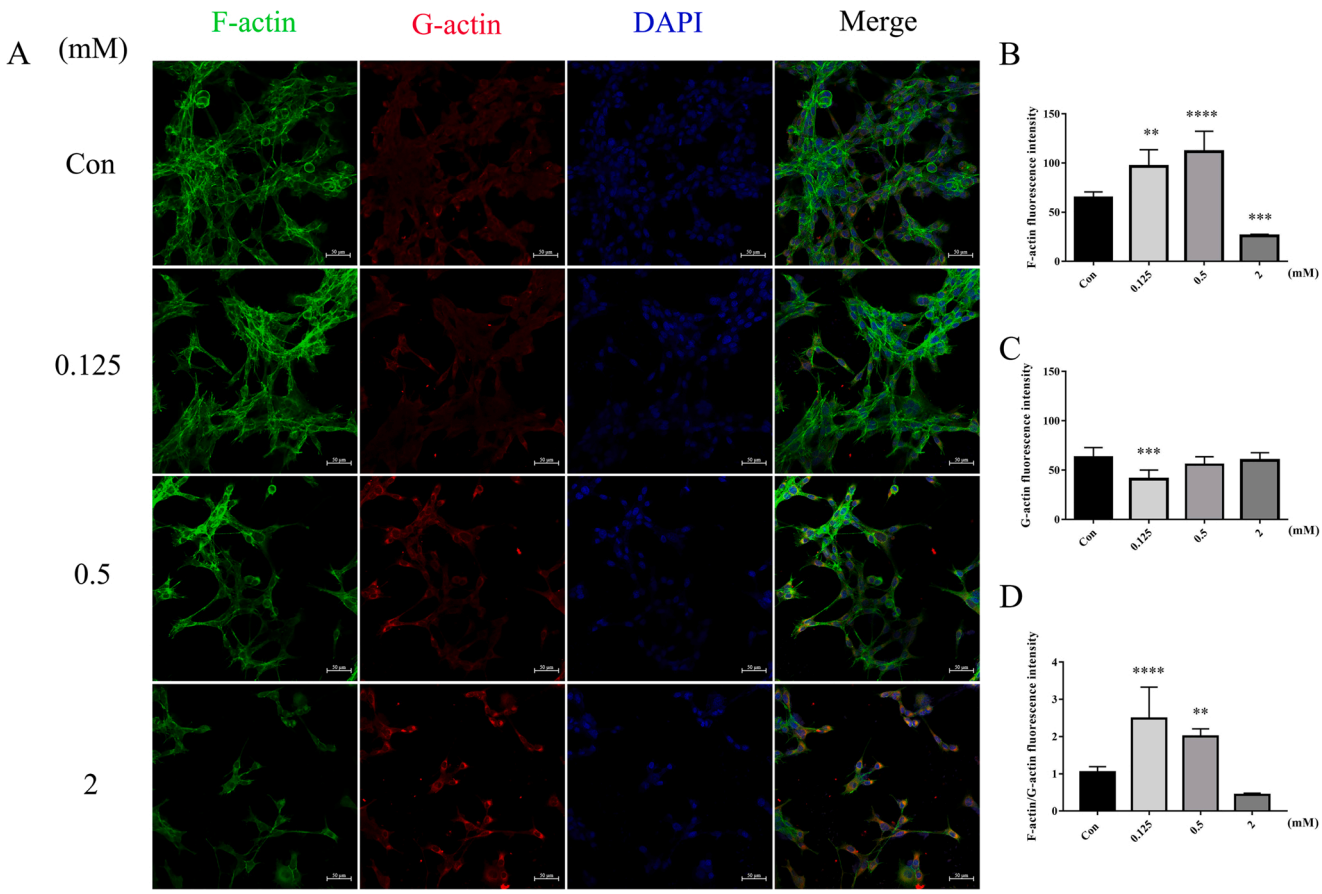

Fig. 5. Fluoride exposure destroys the F-actin/G-actin dynamic balance of HT-22 cells. A: F-actin, G-actin, and DAPI staining. The green label was phalloidin dyed; the red label was DNase I dyed; the blue label was DAPI dyed. B: F-actin fluorescence intensity statistics; C: G-actin fluorescence intensity statistics; D: F-actin/G-actin fluorescence intensity statistics. * *Highly significant differences from control ($p < 0.01$), * **Remarkable significant differences from control ($p < 0.001$), * ** *Extremely significant differences from control ($p < 0.0001$).

PBS. The coverslip was placed on the slide (with an anti-fluorescence inhibitor). Laser confocal microscopy (LSM 800, Zeiss, Germany) was performed, and the results were analyzed using ImageJ software.

2.9. Western blot analysis

The HT-22 cells were harvested after fluoride treatment, and then lysed in ice-cold protein lysis buffer for 30 min and centrifuged at 12,000 rpm for 10 min at 4 ℃. The supernatant was collected. The total protein content of the samples was determined using the BCA protein concentration detection kit (Beyotime Beijing). Equal amounts of (30 μg) protein sample were loaded into a 10% SDS-PAGE gel for separation, transferred onto the PVDF membrane by semi-dry transmembrane instrument (221BR, BIO-RAD) and blocked in 5% non-fat milk for 2 h at room temperature. Then, the membranes were separately incubated with RhoA, ROCK, LIMK, Cofilin, MAP2, Tau, GLUT1, and GLUT3 primary antibodies. Goat anti-mouse or rabbit lgG horseradish peroxidase labeling (ZSbio, Beijing) was used as the secondary antibody. The target bands were detected using super-sensitivity chemiluminescence reagents (Willget biotech, Shanghai China). The ODs of the protein bands were centralized and normalized to GAPDH by using ImageJ software (National Institutes of Health, USA), and results were analyzed using Prism software.

2.10. Quantitative real-time polymerase chain reaction

The total cellular RNA was obtained using TRIzol reagent (Invitrogen, USA) and stored in a refrigerator at −80 °C (Thermo Fisher Scientific, USA). The relative mRNA expression of RhoA, ROCK, LIMK, Cofilin, MAP2, TAU, GLUT1, and GLUT3 were determined using applied biosystems quaint studio 5 (Thermo Fisher Scientific, USA). qRT-PCR was performed in 10 μL of the reaction mixture with the following cycle conditions: 95 ℃ for 30 s, followed by 40 cycles at 95 ℃ for 5 s, 60 ℃ for 20 s, and 72 ℃ for 20 s. The target genes were normalized to the GAPDH, and the mRNA expression was determined using the $2^{-\Delta\Delta Ct}$ method and analyzed using Prism software (Table 1).

2.11. ATP and ATPase content determination

The cells were collected after treatment with fluoride and ground using a frozen grinding instrument (N9548R, Beijing Hide Technology Co., Ltd). Three repetitions were set for each group. ATPase was detected using the ultra-trace ATP enzyme test kit (A070–1, Nanjing Jiancheng, China), ATP content detection used ATP content test kit (A095–1–1, Nanjing Jiancheng, China). ODs were measured by the Multiscan Spectrum at 636 nm and analyzed using Prism software.

2.12. Statistic assay

All the data were expressed as mean ± standard deviation (SD), and set up more than three independent repeats for every group. Results were analyzed using Student's t-test and analysis of variance (ANOVA) by using GraphPad Prism (version 8.3). P values less than 0.05 were considered statistically significant.

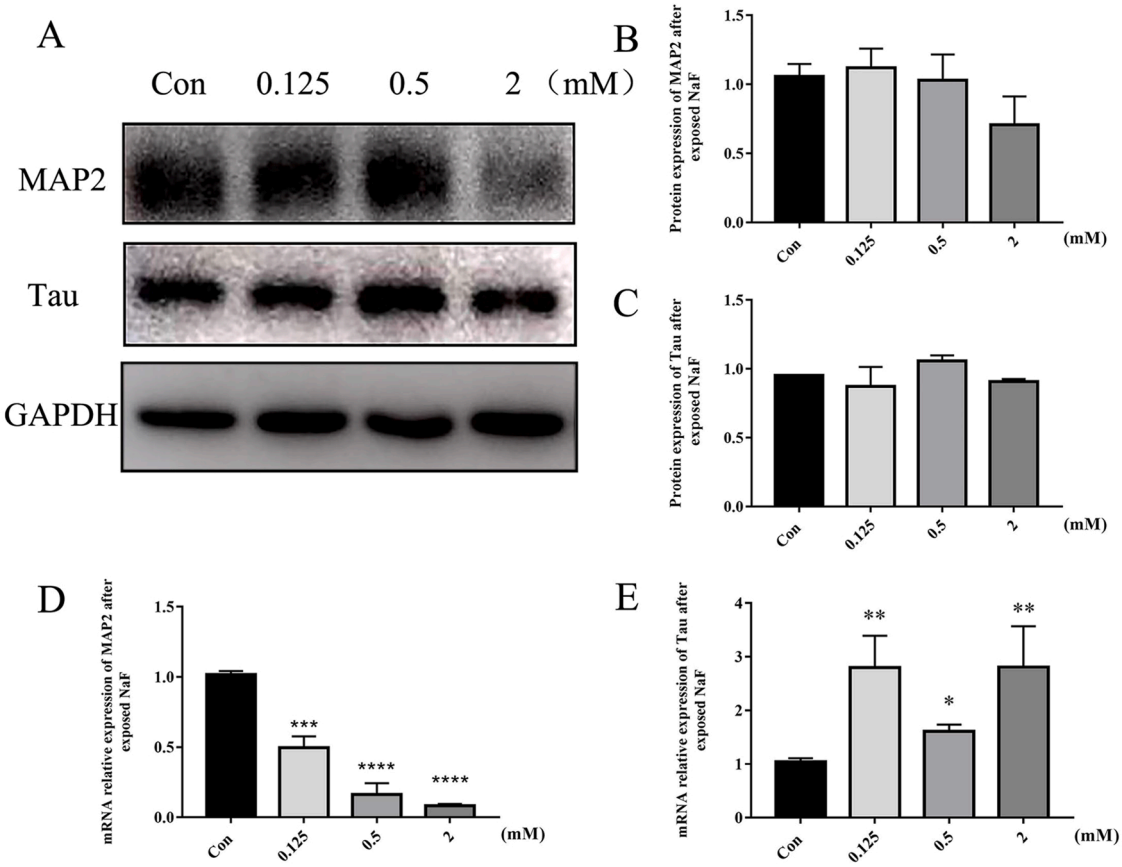

Fig. 6. Expression of MAP2 and Tau in HT-22 cell after fluoride exposure. A: The protein expression of MAP2 and Tau were determined by Western Blot; B: Protein expression of MAP2; C: Protein expression of Tau; D: mRNA expression of MAP2; E: mRNA expression of Tau. *Significantly different from control ($p < 0.05$), * *Highly significant differences from control ($p < 0.01$), **Remarkable significant differences from control ($p < 0.001$), * ** *Extremely significant differences from control ($p < 0.0001$).

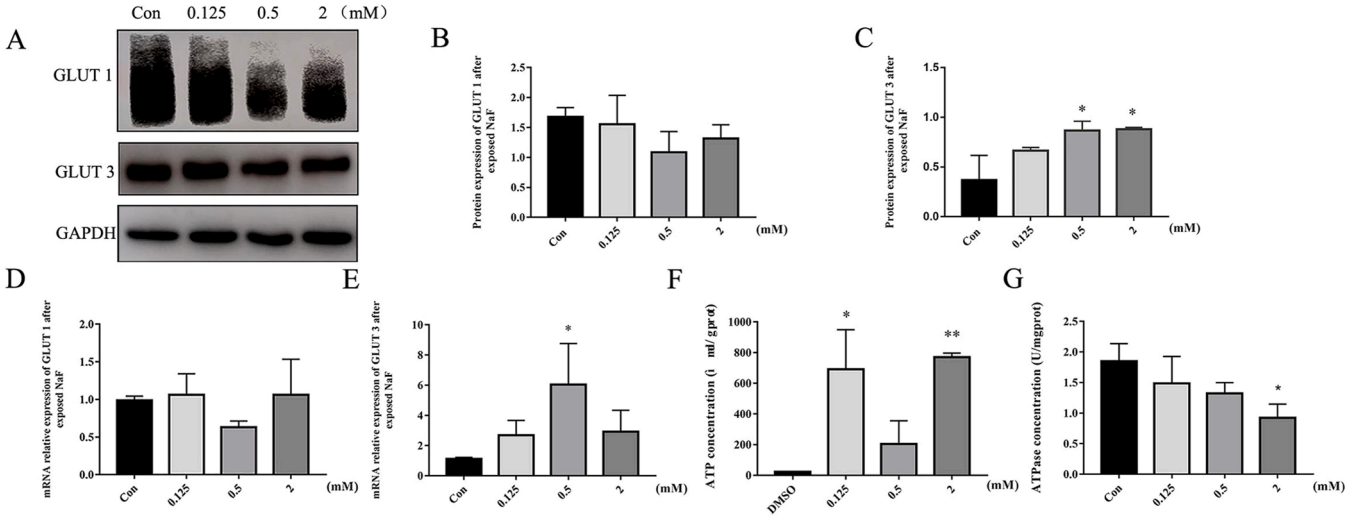

Fig. 7. Determination of the expression of the GLUT1 and GLUT3 and contents of ATP/ATPase in HT-22 cell. A: The proteins expression of GLUT1 and GLUT3 were determined by Western Blot; B: Protein expression of GLUT1; C: Protein expression of GLUT3; D: mRNA expression of GLUT1; E: mRNA expression of GLUT3; F: ATP concentration; G: ATPase concentration. *Significantly different from control ($p < 0.05$), * *Highly significant differences from control ($p < 0.01$).

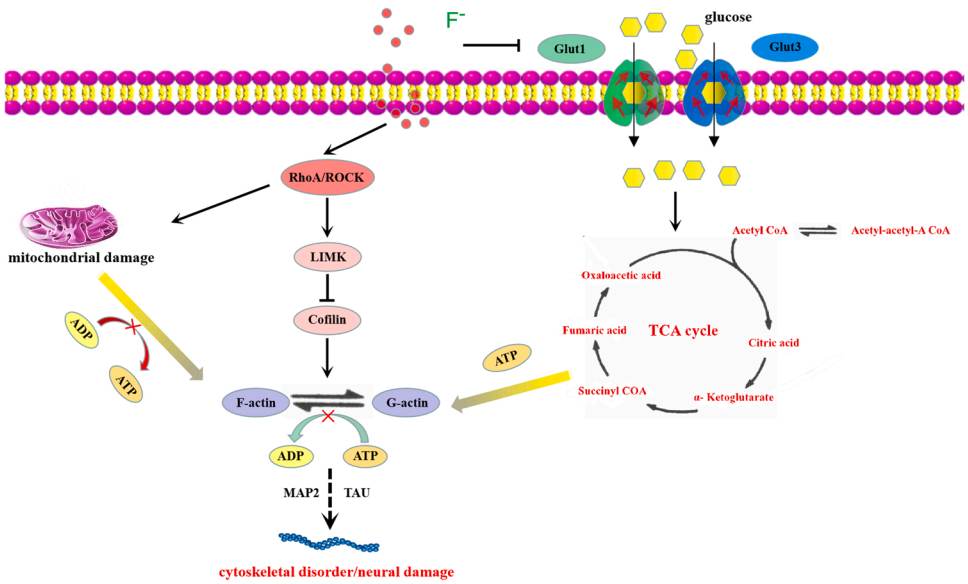

Fig. 8. Mind map of fluoride causing neural damage. Fluoride exposure activates the RhoA/ROCK/LIMK/Cofilin signaling pathway, causing mitochondrial damage. ADP generated ATP reduction. The decreased MAP2 and TAU levels affectes the distribution of the cytoskeleton, thus destroying the dynamic balance of actin and affecting the cellular structure and function. Fluoride affected glucose entry into neurons by affecting GLUT1 and GLUT3. ATP was released through the TCA cycle, thus affecting the transformation of F-actin and G-actin, and the dynamic balance of actin.

3. Results

3.1. NaF depressing proliferation and neurotransmitter release of HT-22 cell

The cell proliferation capacity of HT-22 cells induced by NaF was determined by the CCK-8 kit. As shown in Fig. 1 A, NaF significantly reduced the cell viability in a dose-dependent manner (0.125–10 mM, $p < 0.05$). The IC50 of NaF is 2.079 mM in HT-22 cells, which were assayed by cell counting (Fig. 1 B). Therefore, 0.125, 0.5, and 2 mM were set as ultimate concentrations to explore the cytotoxic effects of NaF in the following experiments.

The optical microscopic observation of HT-22 cells indicated that the cellular morphology and number changed in the fluoride-treated group. In comparison with normal cells cellular bodies became rounder, dendritic spines became shorter, and adhesion decreased gradually after fluoride exposure (Fig. 1 C). Calcein-AM (Fig. 1 D) was used to stain the live cell. The fluorescence intensities were remarkably reduced in the 0.5 and 2 mM fluoride treatment groups ($p < 0.01$), revealing that fluoride attenuated the HT-22 cell viability. LDH is a stable cytoplasmic enzyme, when the cell membrane is damaged, it is quickly released into the cell culture medium. As shown in Fig. 1 E, the LDH content remarkably increased in the 0.5 and 2 mM groups ($p < 0.01$), revealing that NaF increased the membrane permeability of HT-22 cells.

The cytotoxicity detection kit results displayed that the ratio of dead/live cells remarkably increased in fluoride treatment groups with control (Fig. 2 A, B). Fig. 2 C showed that glutamate secreted no distinctness in the fluoride treatment group with control. Therefore, fluoride reduced the proliferation and survival rates of HT-22 cells.

3.2. NaF causes impairment of ultrastructure in HT-22 cell

Fig. 3 showed that in the control group, the microvilli of the cell surface were abundant, the cell membrane was consecutive and complete, the chromatin was evenly distributed, distinct nucleolus are present in the nuclei, and the mitochondrial structure was normal. Microfilament and microtubules are arranged orderly and complete. In the fluoride group, the cells were swelling, microvilli content decreased, cellular membrane integrity was damaged to varying degrees, chromatin was sparse, mitochondria ridge gap became wide, and microfilament and microtubule density were scarce. Therefore, NaF caused the impairment of ultrastructure in HT-22 cells, consisting of increased LDH content.

3.3. NaF activates the RhoA/ROCK/LIMK/Cofilin signaling pathway in HT-22 cell

NaF exposure induced the damage of microfilament and microtubules. Generally, the RhoA/ROCK signaling pathway can regulate the structure and function of the cytoskeleton. However, whether RhoA/ROCK/LIMK/Cofilin signaling pathway participates in the fluoride-induced structural and functional disorder has not been reported. The next studies were used to verify this question by Western Blot and qRT-PCR analysis. The protein expression level of ROCK1 was significantly upregulated in the 2 mM fluoride treatment group ($p < 0.05$), and LIMK was significantly upregulated in the 0.5 and 2 mM fluoride treatment groups ($p < 0.05$). In addition, RhoA and Cofilin expression increased but no remarkable difference (Fig. 4 A, B). Furthermore, qRT-PCR was applied to identify the relative mRNA expression of RhoA, ROCK1/2, LIMK, and Cofilin after fluoride exposure. Higher mRNA expression was found in NaF groups than in the normal cell, but no significant difference (Fig. 4 C). The results revealed that the RhoA/ROCK/LIMK/Cofilin signaling pathway was activated by NaF.

3.4. NaF exposure destroys the actin homeostasis of HT-22 cell

The above results confirm that NaF activated the RhoA/ROCK/LIMK/Cofilin signaling pathway and induced actin realignment. Therefore, the influence of this result on the actin homeostasis (F-actin/G-actin dynamic balance) of the cell needs to be determined. In the present study, DNase I solution and phalloidin were used to mark G-actin and F-actin, respectively. As shown in Fig. 5 A, a large number of cells can be observed under the visual field, F-actin and G-actin uniform distribution of whole cellular bodies with abundant synaptic connections among cells in the control group. By contrast, the number of cells decreased, and F-actin fluorescence intensity significantly increased in the 0.125 and 0.5 mM fluoride treatment group (Fig. 5 B, $p < 0.01$), but significantly decreased in the 2 mM fluoride treatment group ($p < 0.001$). G-actin fluorescence intensity significantly decreased in the 0.125 mM fluoride treatment group (Fig. 5 C, $p < 0.001$). F-actin/G-actin fluorescence intensity ratio significantly increased in the 0.125 and 0.5 mM fluoride treatment group (Fig. 5 D, $p < 0.01$), and no significant difference in 2 mM NaF.

3.5. NaF affects the protein expression of the cytoskeleton in HT-22 cell

The above results confirmed that NaF disrupts the dynamic balance

of F-actin/G-actin and affects cytoskeletal arrangement. To investigate the mechanism of fluoride in cytoskeletal regulation, we detected the expression of MAP2 and Tau. The mRNA relative expression level of MAP2 significantly decreased in the fluoride treatment groups (Fig. 6 D, $p < 0.001$), while the Tau expression significantly increased (Fig. 6 E, $p < 0.05$). In addition, the protein expression of MAP2 and Tau was suppressed after fluoride treatment (Fig. 6 A,B,C). Therefore, NaF can induce cytoskeletal rearrangement by inhibiting the expression of microtubule-associated proteins in HT-22 cells.

3.6. NaF affects the contents of the ATP enzyme and ATP in HT-22 cell

Glucose is the basic and main energy supply source through the blood circulation into each system of the whole body. The main protein GLUT1 and GLUT3 participate in glucose transport from the blood into the brain in humans and animals. F-actin/G-actin dynamic balance is an essential precondition to maintain the cellular structure and functions, and ATP participates in this process. Above results demonstrated that fluoride exposure induced the F-actin/G-actin dynamic to unbalance, but the effect of this change in ATP production and glucose transport process is unclear. As shown in Fig. 7, the mRNA relative expression of GLUT1 increased in the 0.125 and 2 mM fluoride treatment groups and yet decreased in 0.5 mM (Fig. 7 D, $p < 0.05$), while GLUT3 increased in all NaF groups, especially in 0.5 mM fluoride treatment groups (Fig. 7 E, $p < 0.05$). Western Blot analysis results demonstrated that the protein expression of GLUT1 decreased in the treatment groups compared with the control ($p < 0.05$). The protein expression of GLUT3 increased in all fluoride treatment groups, especially in the 0.5 and 2 mM fluoride treatment groups (Fig. 7 A, B, C, $p < 0.05$). ATP assay kit analysis showed the ATP contents significantly increased after fluoride treatment compared with the control (Fig. 7 F, $p < 0.05$). ATPase assay kit analysis showed that the ATP enzyme decreased in the treatment groups, and a significant difference in 2 mM (Fig. 7 G, $p < 0.05$). Therefore, NaF exposure can influence the glucose transport and ATP production process in HT-22 cells.

4. Discussion

Fluorine, a toxic and reactive element, is widespread in the environment and can induce neurotoxicity in humans and animals. Fluoride has a dual impact on human health. The normal growth and development of human teeth and bones require trace amounts of fluoride, while excessive ingestion will cause damage to tissues, organs, and systems (Qiao et al., 2021). Drinking water with a concentration between 0.5 and 1.0 ppm is beneficial to prevent dental caries, while exceeding 1.5 ppm will lead to fluorosis (Srivastava and Flora, 2020). NaF exposure induced the expression of brain-derived neurotrophic factor (BDNF) increased, and glial fibrillary acidic protein (GFAP) decreased in the cerebral cortex and hippocampus of SD rats (Jiang et al., 2014). Results indicate a significantly increased frequency of DNA damage and the synthesis of proinflammatory transcription factors (NF-kB) after fluorine treatment in primary neurons of rat hippocampus (Zhang et al., 2008). However, the neurotoxic mechanism of fluoride is not clear.

Previous studies showed that fluoride exhibited dose-dependent neurotoxicity in vivo and in vitro which can cause ultrastructural damage and downregulated the expression of cytoskeletal protein MAP2 and TAU (Chen et al., 2017; Ning et al., 2021). In our study, CCK-8, and CCK-F assay results indicated that fluoride can significantly reduce cellular proliferation and activity in HT-22 cells. Meanwhile, the TEM showed cellular membrane integrity, mitochondria, microfilament, and microtubules were damaged after fluoride exposure. The LDH test suggested that fluoride increased the membrane permeability of HT-22 cells in a dose-dependent manner. Based on these results, cell morphology changed in the treatment groups compared with the control, but the secretion of neurotransmitter glutamate has no significant difference in HT-22 cells. Therefore, fluoride affects the morphology, vitality, and membrane integrity of HT-22 cells.

Kandimalla et al. reported the changes in the expression of MAP2, one soluble protein, caused by abnormal phosphorylation triggers neurotoxic processes (Kandimalla et al., 2018). Alzheimer's disease (AD) and demyelination (DE) lead to the disassembly of MAP2 and Tau accumulation (Gutiérrez-Vargas et al., 2022). In the present study, results indicated that fluoride causes MAP2 suppressing expression in mRNA level, but Tau showed contradictory trends. In addition, the MAP2 and Tau protein expression had no difference among intergroup. The actin staining result showed that fluoride-induced cytoskeletal arrangement was disorderly and F-actin/G-actin dynamic unbalance. It is widely known that the normal arrangement of the cytoskeleton is crucial for the initial establishment of the polarity of cell (Tahirovic and Bradke, 2009), and various signal molecules of the Rho family are involved in regulating cytoskeletal dynamics (Jaffe and Hall, 2005). The RhoA/ROCK pathway is closely associated with the growth of neurons and their axons. The activation of this pathway may disrupt dendritic spine structure and function, and affect neurite morphology, extension, and growth, which causes axonal growth inhibition, synaptic damage, and synaptic loss (Sellers et al., 2018; Swanger et al., 2016; Bisbal et al., 2018). Rho GTPase-activating protein 35 (ARHGAP35) could directly regulate cytoskeletal reorganization by activating RhoA (Sun et al., 2014). Evidence from animal studies reveals that the RhoA/ROCK signaling pathway is involved in various CNS diseases, such as Alzheimer's disease (Henderson et al., 2016), Parkinson's disease (Iyer et al., 2021), and amyotrophic lateral sclerosis (Günther et al., 2017). RhoA/ROCK is a promising drug target in neurodegenerative diseases. In the present study, fluoride exposure induced the cytoskeletal arrangement, and activates the RhoA/ROCK/LIMK/Cofilin signaling pathway of mRNA and protein in HT-22 cells. We can suggest that fluoride affects the arrangement of the cytoskeleton by the activation of the RhoA/ROCK/LIMK/Cofilin signaling pathway.

GLUT1 is located on the endothelial cells of the blood-brain, and mediates the transport of glucose from the blood to the brain. GLUT3 is ubiquitously and abundantly expressed in brain neurons and serves in the housekeeping uptake of D-glucose into neurons (Koepsell, 2020). The decreased expression levels of GLUT1 and GLUT3 in the cerebral cortex of AD patients, impair glucose uptake in the brain, thus leading to the hyperphosphorylation of Tau protein (Watson and McStay, 2020). Beta-amyloid (Aβ42) caused decreased protein and mRNA expression levels of GLUT1 and GLUT3, ultimately leading to decreased glucose uptake and metabolism in male C57BL/6 J mice and male APP/PS1 transgenic mice. Shen-Zhi-Ling oral liquid reduced GLUT1 but alleviated the decrease in GLUT3 caused by Aβ42, enhancing glucose uptake and metabolism (Qin et al., 2021). The expression of GLUT1 and GLUT3 was upregulated in the colorectal cancer cell line cultured under hypoglycemic or no glucose (Reckzeh et al., 2019). Moreover, in tumor cells, GLUT1 and GLUT3 expression levels were upregulated in response to HIF-1a (Masoud and Li, 2015). In the present study, GLUT1 was reduced, while GLUT3 was significantly increased in the NaF groups of the mRNA and the protein, possibly because of cellular compensation, thus affecting the uptake of glucose.

Adenosine triphosphate (ATP) is within the organism the carrier of energy conversion, and its change will affect the function of cells. Adenosine triphosphatases (ATPase) are found in rhagiocrine cells or membranes of organelles, and they participate in energy transformation and in material and information transportation. ATPases utilize ATP hydrolysis to actively pump substrates across cell membranes and maintain the ionic gradient of cells (Dyla et al., 2020). Mitochondria are the main sites for ATP production in cells, and mitochondrial damage leads to ATP reduction. ATP content increased the transformation from F-actin to G-actin, whereas ATP hydrolysis to ADP restrained the transformation from G-actin to F-actin. Our results showed ATP contents significantly increased, and ATPase significantly decreased after fluoride treatment compared with the control. This finding suggest that fluoride reduces the level of ATPase and the ability of ATP hydrolysis to

ADP decreases, resulting in high ATP content in HT-22 cell.

5. Conclusion

In summary, as shown in the mind map of fluorine causing neural damage (Fig. 8), this study instructed that fluoride activities the RhoA/ROCK/LIMK/Cofilin signaling pathway, thus effect HT-22 cell survival, cellular morphology, and ultrastructure, inhibit neuronal function and perturb the dynamic balance of actin. Moreover, fluoride exposure affects glucose entry into neurons and ATP production by interfering with the expression of GLUT1 and GLUT3, ultimately affecting structure and function of the neuron. These findings provide strong evidence of the neurotoxic mechanism of fluoride. However, the effect of fluoride on synaptic development needs to be further explored.

CRediT authorship contribution statement

Yaming Ge and Lingli Chen conceived and designed the study. **Penghuan Jia, Yuye Liu, and Rui Wang** executed the experiment and analyzed the data. All authors interpreted the data and approved the final version.

Declaration of Competing Interest

The authors declare that they have no known competing financial interests or personal relationships that could have appeared to influence the work reported in this paper.

Data availability

Data will be made available on request.

Acknowledgments

This work was supported by the National Natural Science Foundation of China (32002352), the Scientific and Technological Foundation of Henan Province in China (222102310027 and 222102310382), Key Research Projects in Colleges of Henan province (22A230007 and 23A180019), and Postdoctoral research grant in Henan Province (202101059).

References

Amano, M., Nakayama, M., Kaibuchi, K., 2010. Rho-kinase/ROCK: a key regulator of the cytoskeleton and cell polarity. Cytoskeleton. (Hoboken) 67 (9), 545–554. https://doi.org/10.1002/cm.20472.

Berrou, J., Dupont, M., Djamai, H., Adicéam, E., Parietti, V., Kaci, A., et al., 2022. Preclinical evaluation of a novel small molecule inhibitor of LIM kinases (LIMK) CEL_amide in philadelphia-chromosome positive (BCR::ABL+) acute lymphoblastic leukemia (ALL). J. Clin. Med. Nov. 15 11 (22), 6761. https://doi.org/10.3390/jcm11226761.

Bisbal, Mariano, Remedi, M.ónica, Quassollo, Gonzalo, Cáceres, Alfredo, Sanchez, M.ó nica, 2018. Rotenone inhibits axonogenesis via an Lfc/RhoA/ROCK pathway in cultured hippocampal neurons. J. Neurochem 146 (5), 570–584. https://doi.org/10.1111/jnc.14547.

Brandt, R., Trushina, N.I., Bakota, L., 2020. Much more than a cytoskeletal protein: physiological and pathological functions of the non-microtubule binding region of Tau. Front Neurol. 11, 590059 https://doi.org/10.3389/fneur.2020.590059.

Chen, J., Niu, Q., Xia, T., Zhou, G., Li, P., Zhao, Q., et al., 2018. ERK1/2-mediated disruption of BDNF-TrkB signaling causes synaptic impairment contributing to fluoride-induced developmental neurotoxicity. Toxicology 410, 222–230. https://doi.org/10.1016/j.tox.2018.08.009.

Chen, L., Ning, H., Yin, Z., Song, X., Feng, Y., Qin, H., et al., 2017. The effects of fluoride on neuronal function occurs via cytoskeleton damage and decreased signal transmission. Chemosphere 185, 589–594. https://doi.org/10.1016/j.chemosphere.2017.06.128.

Dec, K., Ukomska, A., Maciejewska, D., Jakubczyk, K., Baranowska-Bosiacka, I., Chlubek, D., et al., 2017. The influence of fluorine on the disturbances of homeostasis in the central nervous system. Biol. Trace Elem. Res 177 (2), 224–234. https://doi.org/10.1007/s12011-016-0871-4.

Dyla, M., Kjærgaard, M., Poulsen, H., Nissen, P., 2020. Structure and mechanism of P-Type ATPase ion pumps. Annu Rev. Biochem 89, 583–603. https://doi.org/10.1146/annurev-biochem-010611-112801.

Günther, R., Black, A., Koch, J.C., Nientiedt, T., Sereda, M., Bähr, M., et al., 2017. Rho Kinase Inhibition with Fasudil in the SOD1G93A Mouse Model of Amyotrophic Lateral Sclerosis-Symptomatic Treatment Potential after Disease Onset. Front Pharm. 8, 17. https://doi.org/10.3389/fphar.2017.00017.

Gutiérrez-Vargas, J.A., Castro-Álvarez, J.F., Zapata-Berruecos, J.F., Abdul-Rahim, K., Arteaga-Noriega, A., 2022. Neurodegeneration and convergent factors contributing to the deterioration of the cytoskeleton in Alzheimer's disease, cerebral ischemia and multiple sclerosis (Review). Biomed. Rep. 16 (4), 27. https://doi.org/10.3892/br.2022.1510.

Hauke, M., Eckenstaler, R., Ripperger, A., Ender, A., Braun, H., Benndorf, R.A., 2022. Active RhoA exerts an inhibitory effect on the homeostasis and angiogenic capacity of human endothelial cells. J. Am. Heart Assoc. 11 (12), e025119 https://doi.org/10.1161/JAHA.121.025119.

Henderson, B.W., Gentry, E.G., Rush, T., Troncoso, J.C., Thambisetty, M., Montine, T.J., et al., 2016. Rho-associated protein kinase 1 (ROCK1) is increased in Alzheimer's disease and ROCK1 depletion reduces amyloid-β levels in brain. J. Neurochem 138 (4), 525–531. https://doi.org/10.1111/jnc.13688.

Iyer, M., Subramaniam, M.D., Venkatesan, D., Cho, S.G., Ryding, M., Meyer, M., et al., 2021. Role of RhoA-ROCK signaling in Parkinson's disease. Eur. J. Pharm. 894, 173815 https://doi.org/10.1016/j.ejphar.2020.173815.

Jaffe, A.B., Hall, A., 2005. RHO GTPASES: biochemistry and biology. Annu Rev. Cell Dev. Biol. 21, 247–269. https://doi.org/10.1146/annurev.cellbio.21.020604.150721.

Jiang, C., Zhang, S., Liu, H., Guan, Z., Zeng, Q., Zhang, C., et al., 2014. Low glucose utilization and neurodegenerative changes caused by sodium fluoride exposure in rat's developmental brain. Neuromolecular Med. 16 (1), 94–105. https://doi.org/10.1007/s12017-013-8260-z.

Kandimalla, R., Manczak, M., Yin, X., Wang, R., Reddy, P.H., 2018. Hippocampal phosphorylated tau induced cognitive decline, dendritic spine loss and mitochondrial abnormalities in a mouse model of Alzheimer's disease. Hum. Mol. Genet 27 (1), 30–40. https://doi.org/10.1093/hmg/ddx381.

Koepsell, H., 2020. Glucose transporters in brain in health and disease. Pflug. Arch. 472 (9), 1299–1343. https://doi.org/10.1007/s00424-020-02441-x.

Lee, D.H., Lee, J.Y., Hong, D.Y., Lee, E.C., Park, S.W., Jo, Y.N., 2022. ROCK and PDE-5 inhibitors for the treatment of dementia: literature review and meta-analysis. Biomed., 10 (6), undefined. https://doi.org/10.3390/biomedicines10061348.

Li, Weisheng, Lu, Likui, Zhu, Dan, et al., 2022. Gestational exposure to fluoride impairs cognition in C57 BL/6 J male offspring mice via the p-Creb1-BDNF-TrkB signaling pathway. Ecotoxicol. Environ. Saf. 239, 113682 https://doi.org/10.1016/j.ecoenv.2022.113682.

Liu, M., Xing, F., Bian, C., Zhao, Y., Zhao, J., Liu, Y., et al., 2019. Letrozole induces worse hippocampal synaptic and dendritic changes and spatial memory impairment than ovariectomy in adult female mice. Neurosci. Lett. 706, 61–67. https://doi.org/10.1016/j.neulet.2019.05.006.

Maher, F., Simpson, I.A., 1994. The GLUT3 glucose transporter is the predominant isoform in primary cultured neurons: assessment by biosynthetic and photoaffinity labelling. Biochem J. 301 (Pt 2), 379–384. https://doi.org/10.1042/bj3010379.

Masoud, G.N., Li, W., 2015. HIF-1a Pathway: Role. Regul. Interv. Cancer Ther. Acta Pharm. Sin. B 5 (5), 378–389. https://doi.org/10.1016/j.apsb.2015.05.007.

Ning, H., Li, C., Yin, Z., Hu, D., Ge, Y., Chen, L., 2021. Fluoride exposure decreased neurite formation on cerebral cortical neurons of SD rats in vitro. Environ. Sci. Pollut. Res Int 28 (37), 50975–50982. https://doi.org/10.1007/s11356-021-13950-2.

Niu, Q., Chen, J., Xia, T., et al., 2018. Excessive ER stress and the resulting autophagic flux dysfunction contribute to fluoride-induced neurotoxicity. Environ. Pollut. 233, 889–899. https://doi.org/10.1016/j.envpol.2017.09.015.

Ohashi, K., 2015. Roles of cofilin in development and its mechanisms of regulation. Dev. Growth Differ. 57 (4), 275–290. https://doi.org/10.1111/dgd.12213.

Ohno, O., Morita, M., Kitamura, K., Teruya, T., Yoneda, K., Kita, M., et al., 2013. Apoptosis-inducing activity of the actin-depolymerizing agent aplyronine A and its side-chain derivatives. Bioorg. Med Chem. Lett. 23 (5), 1467–1471. https://doi.org/10.1016/j.bmcl.2012.12.052.

Oyagbemi, A.A., Adebiyi, O.E., Adigun, K.O., Ogunpolu, B.S., Falayi, O.O., Hassan, F.O., et al., 2020. Clofibrate, a PPAR-α agonist, abrogates sodium fluoride-induced neuroinflammation, oxidative stress, and motor incoordination via modulation of GFAP/Iba-1/anti-calbindin signaling pathways. Environ. Toxicol. 35 (2), 242–253. https://doi.org/10.1002/tox.22861.

Pandey, D., Goyal, P., Bamburg, J.R., Siess, W., 2006. Regulation of LIM-kinase 1 and cofilin in thrombin-stimulated platelets. Blood 107 (2), 575–583. https://doi.org/10.1182/blood-2004-11-4377.

Qiao, L., Liu, X., He, Y., Zhang, J., Huang, H., Bian, W., et al., 2021. Progress of signaling pathways, stress pathways and epigenetics in the pathogenesis of skeletal fluorosis. Int. J. Mol. Sci. 22 (21), 11932. https://doi.org/10.3390/ijms222111932.

Qin, G., Dong, Y., Liu, Z., Gong, Z., Gao, C., Zheng, M., et al., 2021. Correction to: Shen-Zhi-Ling oral liquid ameliorates cerebral glucose metabolism disorder in early AD via insulin signal transduction pathway in vivo and in vitro. Chin. Med 16 (1), 144. https://doi.org/10.1186/s13020-021-00551-x.

Qu, C., Yang, W., Kan, Y., Zuo, H., Wu, M., Zhang, Q., et al., 2022. RhoA/ROCK signaling regulates Drp1-mediated mitochondrial fission during collective cell migration. Front Cell Dev. Biol. 10, 882581 https://doi.org/10.3389/fcell.2022.882581.

Rao, P.V., Pattabiraman, P.P., Kopczynski, C., 2017. Role of the Rho GTPase/Rho kinase signaling pathway in pathogenesis and treatment of glaucoma: Bench to bedside research. Exp. Eye Res 158, 23–32. https://doi.org/10.1016/j.exer.2016.08.023.

Reckzeh, E.S., Karageorgis, G., Schwalfenberg, M., Ceballos, J., Nowacki, J., Stroet, M.C.M., et al., 2019. Inhibition of glucose transporters and glutaminase synergistically impairs tumor cell growth. e25 Cell Chem. Biol. 26 (9), 1214–1228. https://doi.org/10.1016/j.chembiol.2019.06.005.

Reddy, Y.P., Tiwari, S., Tomar, L.K., Desai, N., Sharma, V.K., 2021. Fluoride-induced expression of neuroinflammatory markers and neurophysiological regulation in the brain of wistar rat model. Biol. Trace Elem. Res 199 (7), 2621–2626. https://doi.org/10.1007/s12011-020-02362-x.

Schindler, A., Foley, E., 2013. Hexokinase 1 blocks apoptotic signals at the mitochondria. Cell Signal 25 (12), 2685–2692. https://doi.org/10.1016/j.cellsig.2013.08.035.

Sellers, K.J., Elliott, Christina, Jackson, Joshua, Ghosh, Anshua, Ribe, Elena, Rojo, Ana I., et al., 2018. Amyloid β synaptotoxicity is Wnt-PCP dependent and blocked by fasudil. Alzheimers Dement 14 (3), 306–317. https://doi.org/10.1016/j.jalz.2017.09.008.

Shamah, S.M., Lin, M.Z., Goldberg, J.L., Estrach, S., Sahin, M., Hu, L., et al., 2001. EphA receptors regulate growth cone dynamics through the novel guanine nucleotide exchange factor ephexin. Cell 105 (2), 233–244. https://doi.org/10.1016/s0092-8674(01)00314-2.

Song, H., Zhang, J., He, W., Wang, P., Wang, F., 2019. Activation of cofilin increases intestinal permeability via depolymerization of F-actin during hypoxia in vitro, 1455-1455 Front Physiol. 10. https://doi.org/10.3389/fphys.

Srivastava, S., Flora, S.J.S., 2020. Fluoride in drinking water and skeletal fluorosis: a review of the global impact. Curr. Environ. Health Rep. 7 (2), 140–146. https://doi.org/10.1007/s40572-020-00270-9.

Sun, M., Liu, W., Zhou, M., 2022. ANGPTL7 is transcriptionally regulated by SP1 and modulates glucocorticoid-induced cross-linked actin networks in trabecular meshwork cells via the RhoA/ROCK pathway. Cell Death Disco 8 (1), 50. https://doi.org/10.1038/s41420-022-00847-3.

Sun, Q., Cibas, E.S., Huang, H., Hodgson, L., Overholtzer, M., 2014. Induction of entosis by epithelial cadherin expression. Cell Res. 24 (11), 1288–1298. https://doi.org/10.1038/cr.

Sündermann, F., Fernandez, M.P., Morgan, R.O., 2016. An evolutionary roadmap to the microtubule-associated protein MAP Tau. BMC Genom. 17, 264. https://doi.org/10.1186/s12864-016-2590-9.

Swanger, S.A., Mattheyses, A.L., Gentry, E.G., Herskowitz, J.H., 2016. ROCK1 and ROCK2 inhibition alters dendritic spine morphology in hippocampal neurons. Cell Logist. 5 (4), e1133266 https://doi.org/10.1080/21592799.2015.1133266.

Tahirovic, S., Bradke, F., 2009. Neuronal polarity. Cold Spring Harb. Perspect. Biol. 1 (3), a001644. https://doi.org/10.1101/cshperspect.a001644.

Turner, J.R., 2009. Intestinal mucosal barrier function in health and disease. Nat. Rev. Immunol. 9 (11), 799–809. https://doi.org/10.1038/nri2653.

U.S. Environmental Protection Agency, 2010. Fluoride: Exposure and Relative Source Contribution Analysis. 820–R–10–015. U. S. Environmental Protection Agency,, Washington, DC.

Wang, X., Tewari, N., Sato, F., Tanimoto, K., Thangavelu, L., Makishima, M., et al., 2022. Biphasic Functions of Sodium Fluoride (NaF) in Soft and in Hard Periodontal Tissues. Int J. Mol. Sci. 23 (2), 962. https://doi.org/10.3390/ijms23020962.

Wang, Y.H., Wang, D.W., Wu, N., Wang, Y., Yin, Z.Q., 2012. α-Crystallin promotes rat axonal regeneration through regulation of RhoA/rock/cofilin/MLC signaling pathways. J. Mol. Neurosci. 46 (1), 138–144. https://doi.org/10.1007/s12031-011-9537-z.

Watson, S.A., McStay, G.P., 2020. Functions of Cytochrome c oxidase Assembly Factors. Int J. Mol. Sci. 21 (19), 7254–7267. https://doi.org/10.3390/ijms21197254.

Whelton, H.P., Spencer, A.J., Do, L.G., Rugg-Gunn, A.J., 2019. Fluoride revolution and dental caries: evolution of policies for global use. J. Dent. Res 98 (8), 837–846. https://doi.org/10.1177/0022034519843495.

World Health Organization, 2017. Guidelines for drinking-water quality, Fourth edition.,. incorporating the first addendum, Geneva. 〈http://apps.who.int/iris/bitstream/10665/254637/1/9789241549950-eng〉.

Wu, J., Cheng, M., Liu, Q., Yang, J., et al., 2015. Protective role of tert-butylhydroquinone against sodium fluoride-induced oxidative stress and apoptosis in PC12 cells. Cell Mol. Neurobiol. 35 (7), 1017–1025. https://doi.org/10.1007/s10571-015-0196-4.

Xue, Y., He, J.T., Zhang, K.K., Chen, L.J., Wang, Q., Xie, X.L., 2019. Methamphetamine reduces expressions of tight junction proteins, rearranges F-actin cytoskeleton and increases the blood brain barrier permeability via the RhoA/ROCK-dependent pathway. Biochem Biophys. Res Commun. 509 (2), 395–401. https://doi.org/10.1016/j.bbrc.2018.12.144.

Yamaguchi, H., Condeelis, J., 2007. Regulation of the actin cytoskeleton in cancer cell migration and invasion. Biochim Biophys. Acta 1773 (5), 642–652. https://doi.org/10.1016/j.bbamcr.2006.07.001.

Yan, N., Liu, Y., Liu, S., et al., 2016. Fluoride-induced neuron apoptosis and expressions of inflammatory factors by activating microglia in rat brain. Mol. Neurobiol. 53 (7), 4449–4460. https://doi.org/10.1007/s12035-015-9380-2.

Zhang, M., Wang, A., Xia, T., He, P., 2008. Effects of fluoride on DNA damage, S-phase cell-cycle arrest and the expression of NF-kappaB in primary cultured rat hippocampal neurons. Toxicol. Lett. 179 (1), 1–5. https://doi.org/10.1016/j.toxlet.2008.03.002.

Zhang, Y., Qian, Y., Li, W., Gao, X., Pan, B., 2019. Fluoride uptake by three lanthanum based nanomaterials: behavior and mechanism dependent upon lanthanum species. Sci. Total Environ. 683, 609–616. https://doi.org/10.1016/j.scitotenv.2019.05.185.

Zhou, C.Y., Wang, Y., Pan, D.D., Sun, Y.Y., Cao, J.X., 2018. The effect of ATP marination on the depolymerization of actin filament in goose muscles during postmortem conditioning. Poult. Sci. 97 (2), 684–694. https://doi.org/10.3382/ps/pex318.

Zhu, W., Zhang, J., Zhang, Z., 2011. Effects of fluoride on synaptic membrane fluidity and PSD-95 expression level in rat hippocampus. Biol. Trace Elem. Res 139 (2), 197–203. https://doi.org/10.1007/s12011-010-8654-9.

Zhu, Y.P., Xi, S.H., Li, M.Y., et al., 2017. Fluoride and arsenic exposure affects spatial memory and activates the ERK/CREB signaling pathway in offspring rats. Neurotoxicology 59, 56–64. https://doi.org/10.1016/j.neuro.2017.01.006.